Available online at www.sciencedirect.com
SCIENCE DIRECT®
Journal of the Mechanics and Physics of Solids
53 (2005) 1827–1854
JOURNAL OF THE MECHANICS AND PHYSICS OF SOLIDS
www.elsevier.com/locate/jmps

Surface free energy and its effect on the elastic behavior of nano-sized particles, wires and films

Rémi Dingreville[a], Jianmin Qu[a,*], Mohammed Cherkaoui[b]

[a]*School of Mechanical Engineering, Georgia Institute of Technology, Atlanta, GA 30332-0405, USA*
[b]*Department of Mechanical Engineering, LPMM-CNRS, ISGMP, University of Metz, Ile du Saulcy, 57045, Metz Cedex1, France*

Received 14 October 2004; accepted 25 February 2005

Abstract

Atoms at a free surface experience a different local environment than do atoms in the bulk of a material. As a result, the energy associated with these atoms will, in general, be different from that of the atoms in the bulk. The excess energy associated with surface atoms is called surface free energy. In traditional continuum mechanics, such surface free energy is typically neglected because it is associated with only a few layers of atoms near the surface and the ratio of the volume occupied by the surface atoms and the total volume of material of interest is extremely small. However, for nano-size particles, wires and films, the surface to volume ratio becomes significant, and so does the effect of surface free energy. In this paper, a framework is developed to incorporate the surface free energy into the continuum theory of mechanics. Based on this approach, it is demonstrated that the overall elastic behavior of structural elements (such as particles, wires, films) is size-dependent. Although such size-dependency is negligible for conventional structural elements, it becomes significant when at least one of the dimensions of the element shrinks to nanometers. Numerical examples are given in the paper to illustrate quantitatively the effects of surface free energy on the elastic properties of nano-size particles, wires and films.

Keywords: Surface energy; Surface stress; Nano-fiber; Nano-wire; Nano-film

*Corresponding author. Tel.: +1 4048945687; fax: +1 4048940186.
E-mail address: jianmin.qu@me.gatech.edu (Jianmin Qu).

0022-5096/$ - see front matter © 2005 Elsevier Ltd. All rights reserved.
doi:10.1016/j.jmps.2005.02.012

1. Introduction

Nanomaterials in general can be roughly classified into two categories. If the characteristic length of the microstructure, such as the grain size of a polycrystal, is in the nanometer range, it is called a nano-structured material. If at least one of the overall dimensions of a structural element is in the nanometer range, it may be called a nano-sized structural element. This may include nano-particles (Alymov and Shorshorov, 1999; Pei and Hwang, 2003), nano-belts (Pan et al., 2001), nano-wires, nano-films, etc. Clearly, nano-sized structural elements must, by necessity, be made of nano-structured materials.

This paper is primarily concerned with the elastic behavior of nano-sized structural elements such as nano-particles, nano-wires and nano-films. In particular, the size dependency of the overall elastic behavior of such nano-sized structural elements will be investigated.

The elastic behavior of a material is characterized by its elastic modulus, which defines the proportionality between the stress and strain when the material is subjected to external loads. Strictly speaking, modulus is an intensive property defined at each material point when the material is assumed to be a continuum. Therefore, it should be independent of the size of the material sample being considered. However, for inhomogeneous materials such as composites, it is often convenient for engineering design to define the overall (or effective) modulus of the material. Such effective modulus of a composite may depend on the properties of its constituents and the relative volume fraction of each constituent.

The reduced coordination of atoms near a free surface induces a corresponding redistribution of electronic charge, which alters the binding situation (Sander, 2003). As a result, the energy of these atoms will, in general, be different from that of the atoms in the bulk. Thus, the elastic moduli of the surface region may differ from those of the bulk. In this sense, all structural elements (large or small), are not strictly homogeneous. However, the surface region is typically very thin, only a few atomic layers. It is thus perfectly acceptable to neglect the surface region and to use the bulk modulus of a structural element as its overall modulus, when the size of the element is in micrometers or larger. For nano-sized structural elements, however, the surface-to-volume ratio is much higher and the surface region can no longer be neglected when considering the overall elastic behavior of nano-sized structural elements. Consequently, the effective modulus of nano-sized structural elements should be considered, and by definition becomes size-dependent.

To include the surface region in modeling nano-sized structural elements inevitably involves discrete (or atomistic) analysis because the boundary region is only a few atomic layers thick. So, one of the fundamental issues that needs to be addressed in modeling the macroscopic mechanical behavior of nano-sized structural elements is the large difference in length scales. To establish a link between the atomistic structure of surfaces and macroscopic bulk elastic behavior, we propose a two-step approach. First, the surface atomistic structure and interactions should be captured and cast into surface free energy, a thermodynamic quantity of a continuum. Then, this surface free energy will be included in the phenomenological

description of strain energy density in modeling the macroscopic behavior of nano-sized structural elements. The surface energy calculation based on molecular dynamics will be presented in a separate paper (Dingreville et al., 2005). In the present paper, we focus on the second step, namely, developing a continuum framework that incorporates the surface free energy into the analysis of macroscopic deformation of nano-sized structural elements. In particular, we study the effects of surface free energy on the effective modulus of nano-particles, nano-wires and nano-films.

Previous work most relevant to this paper is the study on surface and interface stress effects in thin films. It has been found (Cammarata and Sieradzki, 1989, 1994; Kosevich and Kosevich, 1989; Banerjea and Smith, 1987; Nix and Gao, 1998) that the surface free energy could increase the apparent in-plane bi-axial modulus of a Cu (1 0 0) free standing film of 2 nm thick by about 15–25%. Some experimental work (Catlin and Walter, 1960) seems to indicate that the modulus enhancement could be as much as 50%, although it has been pointed out by later studies (Itozaki, 1982; Baker et al., 1993) that such a large enhancement might be due to experimental errors. When the thickness reduces to below 5 nm, modulus enhancement/reduction of 20% was also predicted (Streitz et al., 1994a, b; Cammarata and Sieradzki, 1989) and confirmed experimentally for several multilayered metal films such as Cu–Nb (Fartash et al., 1991). More recently, Miller and Shenoy (2000) developed a simple model to incorporate surface stress in determining the size-dependent elastic modulus of plates and rods. Using molecular dynamic simulations, Zhou and Huang (2004) have shown that, depending upon the crystallographic orientations, the effective elastic modulus of a thin free-standing film can either increase or decrease as the film thickness decreases. The effect of surface stress on the growth of thin films has been investigated by several researchers (e.g., Cammarata, 1997; Nix and Clemens, 1999; Cammarata et al., 2000).

Another relevant area of research is the examination of elastic properties of grain boundaries. A number of publications have suggested that the elastic moduli in the grain boundary domain may differ significantly from those of the bulk. Wolf and co-workers (Wolf et al., 1989; Wolf and Lutsko, 1989; Kluge et al., 1990; Wolf and Kluge, 1990), who studied superlattices of (0 0 1) twist boundaries, as well as Adams et al. (1989), who examined the $\Sigma = 5(0\,0\,1)$ twist boundary in a thin film of copper, have found an increase of the Young's modulus perpendicular to the boundary plane and a substantial decrease of the shear modulus in the boundary plane in the atomic layers adjacent to the boundary. Bassani and co-workers (Alber et al., 1992; Bassani et al., 1992; Vitek et al., 1994; Marinopoulos et al., 1998) defined the local elastic modulus tensor and determined the values of the local elastic modulus tensor near grain boundaries in several face center cubic metals using molecular dynamic simulations. They, too, found that the local elastic moduli are significantly different for atoms near the grain boundaries.

Since grain boundaries have distinct elastic properties, the effective modulus of polycrystalline materials should also be dependent on the grain size because the interface-(grain boundary) to-volume ratio is inversely proportional to the grain size. Unlike the thin film case, however, existing literature has shown mixed results on the

dependency of modulus on grain sizes. Some have reported reduction of elastic modulus by as much as 30% (Suryanarayana, 1995; Gleiter, 1989; Korn et al., 1988) for nano-structured materials. Others (e.g., Nieman et al., 1991; Krstic et al., 1993; Fougere et al., 1995) argued that such reduction is purely due to porosities. However, careful molecular dynamic simulations of copper polycrystal (Schiøtz et al., 1998) have shown that the Young's modulus is indeed reduced by over 25% when the grain size is reduced to 5 nm, even when the polycrystal is fully dense. Similar reduction is seen in simulations where the nanocrystalline metal is grown from a molten phase (Phillpot et al., 1995).

It should be mentioned in passing that an elegant mathematical theory incorporating surface stress and interfacial energy into the continuum mechanics formulation was proposed in the 1970s by Gurtin and his co-workers (e.g., Gurtin and Murdoch, 1975, 1978; Murdoch, 1976; Gurtin et al., 1998). Based on this theory, Sharma and Ganti (2003) have developed the size-dependent Eshelby's tensor for embedded nano-inclusions incorporating interfacial energy. The size-dependent effective modulus of an elastic matrix containing spherical nano-cavities at dilute concentration was obtained by Yang (2004).

2. Surface free energy and surface stress

There are different ways in which the properties of the surface can be defined and introduced. For example, if one considers an "interface" separating two otherwise homogeneous phases, the interfacial property may be defined either in terms of an *inter-phase*, or by introducing the concept of a *dividing surface*. In the first approach, the system is considered to be one in which there are three phases present—the two bulk phases and an inter-phase; the boundaries of the inter-phase are somewhat arbitrary and are usually chosen to be at locations at which the properties are no longer varying significantly with position. The inter-phase then has a finite volume and may be assigned thermodynamic properties in the normal way (e.g., Capolungo et al., 2005, 2005). In the second approach where a single dividing surface is used to separate the two homogeneous phases, the interface contribution to the thermodynamic properties is defined as the excess over the values that would obtain if the bulk phases retained their properties constant up to an imaginary surface (of zero thickness) separating the two phases. In this paper, we adopt this second approach.

The concept of a dividing surface was first introduced by Gibbs (1928) through the use of Gibbs surface free energy (also called surface tension in some literature). The Gibbs density of surface free energy, γ, is defined as the reversible work involved in creating a unit area of *new* surface at constant temperature, volume, and total number of moles. To further illustrate the concept of surface free energy density for a discrete system, consider a representative volume near the surface of a bulk crystal as shown in Fig. 1(a). For simplicity, assume the surface is flat and homogeneous. Results derived under these assumptions remain valid for non-planar surfaces provided that the radius of curvature is significantly greater than the width of the transition region, which is typically a few atomic layer thick (Blakely, 1973).

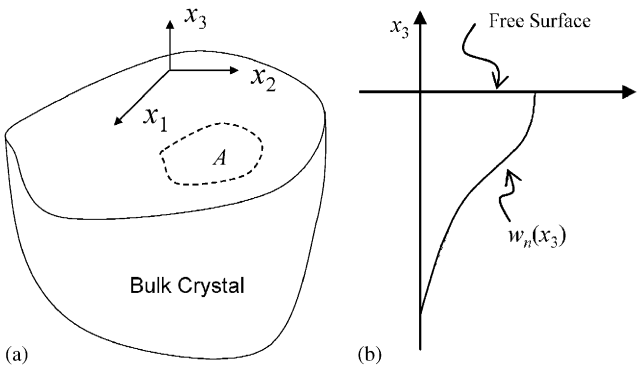

Fig. 1. (a) Free surface of a bulk crystal and (b) surface free energy as a function of the distance away from the surface.

The surface free (excess) energy, w_n, of a near-surface atom is defined by the difference between its total energy and that of an atom deep in the interior of a large crystal. Clearly, w_n depends on the location of the atom. For the crystal surface shown in Fig. 1(a), the x_3-dependence of w_n is schematically shown in Fig. 1(b), i.e., it reaches its maximum value on the surface and tends to zero deep into the crystal. In addition, w_n is a function of the intrinsic crystal surface properties, as well as the relative surface deformation. If there are N atoms underneath an area A, see Fig. 1(a), then the total surface free energy associated with area A is given by $\sum_{n=1}^{N} w_n$. Thus, the Gibbs surface free energy density is defined by

$$\gamma = \frac{1}{A}\sum_{n=1}^{N} w_n. \tag{1}$$

Note that the above definition is in the deformed configuration. It can be viewed as the Eulerian description of the surface free energy density. For solid crystal surfaces, the Lagrange description of the surface free energy density can be defined by

$$\Gamma = \frac{1}{A_0}\sum_{n=1}^{N} w_n, \tag{2}$$

where A_0 is the area originally occupied in the undeformed configuration by the same atoms that occupy the area A in the deformed configuration. It can be easily shown that the two areas are related through

$$A = A_0(1 + \varepsilon^{\mathrm{s}}_{\eta\eta}), \tag{3}$$

where $\varepsilon^{\mathrm{s}}_{\alpha\beta}$ is the Lagrange surface strain relative to the undeformed crystal lattice. Continuity of the strain field requires, for example, in the particular coordinate system shown in Fig. 1(a),

$$\varepsilon^{\mathrm{s}}_{\alpha\beta} = \varepsilon_{\alpha\beta}\big|_{x_3=0}, \quad \alpha,\beta = 1,2,$$

where ε_{ij} is the bulk Lagrange strain of the crystal under a given external loading. In the above and the rest of this paper, Roman indices range from 1 to 3 and Greek indices range from 1 to 2, unless otherwise indicated. For future reference, the Lagrangian strain measure will be used in this paper.

Having defined the surface free energy density, one can now introduce the concept of surface stress. Surface free energy corresponds to the work of creating a unit area of surface, whereas surface stress is involved in computing the work in deforming a surface. Specifically, the change in surface free energy should be equal to the work done by the surface stress as it deforms the surface area, i.e.,

$$\mathrm{d}(\Gamma A_0) = A_0 \Sigma^{\mathrm{s}}_{\alpha\beta}\, \mathrm{d}\varepsilon^{\mathrm{s}}_{\alpha\beta}, \tag{4}$$

where $\Sigma^{\mathrm{s}}_{\alpha\beta}$ is the second Piola–Kirchhoff surface stress tensor. It thus follows that

$$\Sigma^{\mathrm{s}}_{\alpha\beta} = \frac{\mathrm{d}\Gamma}{\mathrm{d}\varepsilon^{\mathrm{s}}_{\alpha\beta}}. \tag{5}$$

This can be considered as the Lagrange description of the well-known Shuttleworth (1950) relation.

Now consider the total surface free energy of a given surface. Let S be the surface area after the deformation, and S_0 be the corresponding area in the undeformed crystal lattice. It then follows from Eq. (4) that the total strain energy stored in the deformed surface is given by

$$U_{\mathrm{surface}} = \int_{S_0} \left[\int_0^{\varepsilon^{\mathrm{s}}_{\alpha\beta}} \Sigma^{\mathrm{s}}_{\alpha\beta}(e_{\kappa\lambda})\, \mathrm{d}e_{\alpha\beta} \right] \mathrm{d}S_0, \tag{6}$$

where $\varepsilon^{\mathrm{s}}_{\alpha\beta}$ is the surface strain in the final deformed configuration, $e_{\alpha\beta}$ is the integration variable representing the surface strain, and the fact that the surface stress is a function of the surface strain is explicitly indicated.

Assuming the surface free energy density is a smooth function of the surface strain, one may expand the surface free energy density into power a series of surface strain, $\varepsilon^{\mathrm{s}}_{\alpha\beta}$,

$$\begin{aligned} \Gamma(\varepsilon^{\mathrm{s}}_{\alpha\beta}) &= \Gamma_0 + \frac{\partial \Gamma}{\partial \varepsilon^{\mathrm{s}}_{\alpha\beta}}\, \varepsilon^{\mathrm{s}}_{\alpha\beta} + \frac{1}{2}\, \frac{\partial^2 \Gamma}{\partial \varepsilon^{\mathrm{s}}_{\alpha\beta} \partial \varepsilon^{\mathrm{s}}_{\kappa\lambda}}\, \varepsilon^{\mathrm{s}}_{\alpha\beta} \varepsilon^{\mathrm{s}}_{\kappa\lambda} + \frac{1}{6}\, \frac{\partial^3 \Gamma}{\partial \varepsilon^{\mathrm{s}}_{\alpha\beta} \partial \varepsilon^{\mathrm{s}}_{\kappa\lambda} \partial \varepsilon^{\mathrm{s}}_{\gamma\eta}}\, \varepsilon^{\mathrm{s}}_{\alpha\beta} \varepsilon^{\mathrm{s}}_{\kappa\lambda} \varepsilon^{\mathrm{s}}_{\gamma\eta} \cdots \\ &= \Gamma_0 + \Gamma^{(1)}_{\alpha\beta} \varepsilon^{\mathrm{s}}_{\alpha\beta} + \frac{1}{2}\, \Gamma^{(2)}_{\alpha\beta\kappa\lambda} \varepsilon^{\mathrm{s}}_{\alpha\beta} \varepsilon^{\mathrm{s}}_{\kappa\lambda} + \frac{1}{6}\, \Gamma^{(3)}_{\alpha\beta\kappa\lambda\gamma\eta} \varepsilon^{\mathrm{s}}_{\alpha\beta} \varepsilon^{\mathrm{s}}_{\kappa\lambda} \varepsilon^{\mathrm{s}}_{\gamma\eta} \cdots, \end{aligned} \tag{7}$$

where Γ_0, $\Gamma^{(1)}_{\alpha\beta}, \cdots$ are material and surface dependent. For a given material surface, they can be either measured experimentally or computed using atomistic simulations (Ackland and Finnis, 1986). Their values computed using molecular dynamic simulation will be reported in a separate publication (Dingreville et al., 2005) for some common materials. Because of symmetry, one has $\Gamma^{(1)}_{\alpha\beta} = \Gamma^{(1)}_{\beta\alpha}$, $\Gamma^{(2)}_{\alpha\beta\kappa\lambda} = \Gamma^{(2)}_{\kappa\lambda\alpha\beta} = \Gamma^{(2)}_{\beta\alpha\kappa\lambda}$ and $\Gamma^{(3)}_{\alpha\beta\kappa\lambda\gamma\eta} = \Gamma^{(3)}_{\beta\alpha\kappa\lambda\gamma\eta} = \Gamma^{(3)}_{\kappa\lambda\alpha\beta\gamma\eta} = \Gamma^{(3)}_{\kappa\lambda\gamma\eta\alpha\beta}$. These conditions imply that there are at most three independent parameters in $\Gamma^{(1)}_{\alpha\beta}$, six in $\Gamma^{(2)}_{\alpha\beta\kappa\lambda}$ and eighteen in $\Gamma^{(3)}_{\alpha\beta\kappa\lambda\gamma\eta}$.

Substitution of Eq. (7) into Eq. (5) yields,

$$\Sigma^{s}_{\alpha\beta} = \Gamma^{(1)}_{\alpha\beta} + \Gamma^{(2)}_{\alpha\beta\kappa\lambda}\varepsilon^{s}_{\kappa\lambda} + \tfrac{1}{2}\Gamma^{(3)}_{\alpha\beta\kappa\lambda\gamma\eta}\varepsilon^{s}_{\kappa\lambda}\varepsilon^{s}_{\gamma\eta}. \tag{8}$$

Clearly, $\Gamma^{(1)}_{\alpha\beta} = \Gamma^{(1)}_{\beta\alpha}$ gives the internal stress of the surface. It represents the part of surface stress that exists even when the surface strain is absent (i.e., when the surface atoms remain in their positions as if they were deep inside a large crystal). The two-dimensional fourth-order tensor $\Gamma^{(2)}_{\alpha\beta\kappa\lambda} = \Gamma^{(2)}_{\kappa\lambda\alpha\beta} = \Gamma^{(2)}_{\beta\alpha\kappa\lambda} = \Gamma^{(2)}_{\alpha\beta\lambda\kappa}$ represents the surface elasticity tensor, while the two-dimensional sixth-order tensor $\Gamma^{(3)}_{\alpha\beta\kappa\lambda\gamma\eta}$ can be viewed as the tensor of the third-order elastic constants of the surface.

Another important comment that must be made here is that both surface free energy density and surface stress are macroscopic thermodynamic quantities. The basic idea of Gibbs surface energy is based on the concept of a dividing surface that separates the two adjacent phases. Under this assumption, the surface contributions to the thermodynamic quantities (e.g., surface free energy and surface stress) are defined as the excesses over the values that would obtain if the bulk phases retained their properties constant up to the dividing surface. In other words, the interface (not interphase) is a mathematical surface of zero thickness over which the thermodynamic properties change discontinuously from one bulk phase to the other. The excess amount is associated only with the dividing surface. Obviously, this is only an idealization of the realistic situation. In the case of a free surface, for example, contributions to the surface free energy come from several layers of atoms near the surface. Molecular dynamics simulations show that free surface induced lattice distortion extends about three layers of atoms into the bulk. So, strictly speaking, the surface free energy derives from not only atoms at the free surface, but also other atoms near the surface. The idealization of the dividing surface is thus valid if and only if the bulk crystal is much larger than several atomic sizes. If the bulk crystal contains only a small number of atoms, the validity of macroscopic thermodynamic quantities such as surface free energy is questionable.

To close this section, we note that deformation in an elastic solid due to surface stresses has been studied quite extensively. Although not explicitly related to surface free energy, Gurtin and Murdoch (1975, 1978), and Gurtin et al. (1998) have developed a continuum framework for elastic surfaces of solids.

3. Effective modulus of a particle

Conventionally, the elastic modulus of a material is an intensive property. It is defined as a point-wise quantity that relates the stresses and strains at each point in the material. When a material is not homogeneous, such as a composite material, its elastic modulus may vary from point to point. In this case, the concept of effective modulus can be introduced. For example, effective modulus is used to characterize the overall stiffness of a fiber reinforced composite, where the fiber and matrix have different elastic moduli.

Now consider a particle made of a single-phase material. On or near the particle surface, the atomistic structure is somewhat different from that of the bulk. Therefore, a particle of a single-phase material, strictly speaking, is not a homogeneous body. The overall stiffness of the particle needs to be characterized by its effective modulus. However, when the particle size is large enough, the surface region is negligible in comparison to the particle volume. In this case, the surface region can be neglected and the particle can be considered as a homogeneous body. Therefore, its elastic modulus is uniform and is the same as that of the material from which the particle is made. This is no longer the case when the particle size shrinks to the nanometer range, where the surface region becomes significant in comparison to the particle size. Consequently, the particle must be viewed as an inhomogeneous body, and the effective modulus of the particle needs to be used to characterize the stiffness of the particle. In this section, a formulation is developed to compute the effective modulus of a particle that incorporates the effect of its surface.

To this end, consider a perfect crystal of infinite extent. Within the infinite crystal, let Ω be an ellipsoidal region consisting of a certain number of atoms. Let the initial volume of Ω be V_0, and its surface area be S_0. Now imagine that Ω is removed from the infinite crystal to become a stand-alone particle, as shown in Fig. 2. The newly created surface of the particle gives rise to surface stresses. Consequently, the particle may deform. The self-equilibrium state of the particle will be discussed later in this section. For now, simply let $\hat{V}$ and $\hat{S}$ be the volume and surface area, respectively, of the particle in its self-equilibrium state.

To describe the deformation of the particle, let us introduce a uniform strain ε_{ij} in the bulk of the particle, where ε_{ij} is measured from the perfect lattice of an undeformed crystal of infinite extent. For an ellipsoidal particle, see Fig. 3, the surface strain is related to the absolute bulk strain within the particle through a coordinate transformation

$$\varepsilon^{s}_{\alpha\beta} = t_{\alpha i} t_{\beta j} \varepsilon_{ij}|_{S}, \tag{9}$$

where the transformation tensor $t_{\alpha i}$ for the ellipsoidal surface is derived in Appendix A.

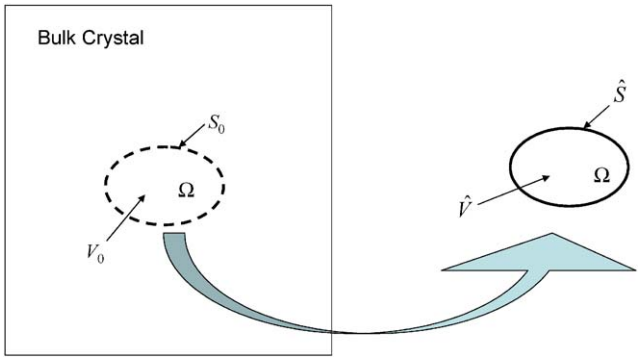

Fig. 2. A particle is created by removing it from a bulk crystal.

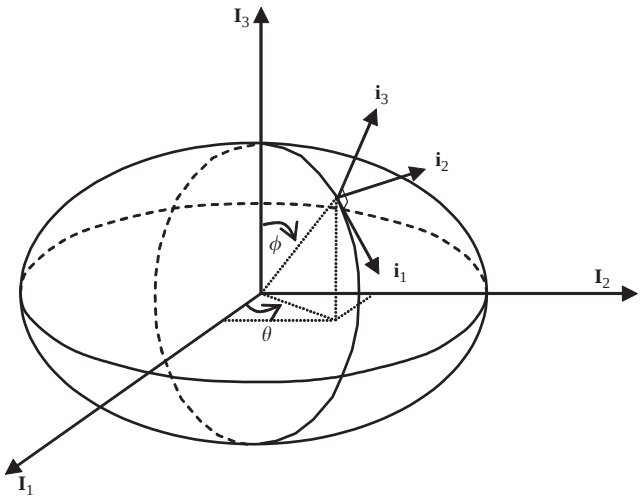

Fig. 3. An ellipsoidal particle.

The total strain energy of the particle corresponding to ε_{ij} can then be written as,

$$U = U_{\text{bulk}} + U_{\text{surface}}, \tag{10}$$

where U_{bulk} is the total strain energy in the bulk of the particle,

$$U_{\text{bulk}} = \int_{V_0} \int_0^{\varepsilon_{ij}} \frac{\partial \Phi}{\partial e_{ij}} \, \mathrm{d}e_{ij} \, \mathrm{d}V_0 = \int_{V_0} [\Phi(\varepsilon_{ij}) - \Phi(0)] \, \mathrm{d}V_0, \tag{11}$$

where Φ is the bulk elastic potential, which can be expanded into a series of the bulk strain tensor,

$$\Phi = \tfrac{1}{2} C_{ijkl} \varepsilon_{ij} \varepsilon_{kl} + \tfrac{1}{6} C^{(3)}_{ijklmn} \varepsilon_{ij} \varepsilon_{kl} \varepsilon_{mn} + \cdots, \tag{12}$$

where C_{ijkl} and $C^{(3)}_{ijklmn}$ are, respectively, the tensors of second- and third-order elastic constants of the perfect crystal lattice. Substituting Eq. (12) into Eq. (11) and neglecting higher order of strains leads to

$$U_{\text{bulk}} = V_0 \left[\tfrac{1}{2} C_{ijkl} \varepsilon_{ij} \varepsilon_{kl} + \tfrac{1}{6} C^{(3)}_{ijklmn} \varepsilon_{ij} \varepsilon_{kl} \varepsilon_{mn} \right]. \tag{13}$$

The total surface free energy on the entire particle surface follows from Eq. (6),

$$U_{\text{surface}} = \int_{S_0} \left[\int_0^{\varepsilon^{\text{s}}_{\alpha\beta}} \Sigma^{\text{s}}_{\alpha\beta}(e_{\kappa\lambda}) \, \mathrm{d}e_{\alpha\beta} \right] \mathrm{d}S_0. \tag{14}$$

Substituting Eq. (5) into Eq. (14) yields,

$$U_{\text{surface}} = \int_{S_0} \left[\int_0^{\varepsilon^{\text{s}}_{\alpha\beta}} \frac{\mathrm{d}\Gamma}{\mathrm{d}e_{\alpha\beta}} \, \mathrm{d}e_{\alpha\beta} \right] \mathrm{d}S_0 = \int_{S_0} [\Gamma(\varepsilon^{\text{s}}_{\alpha\beta}) - \Gamma(0)] \, \mathrm{d}S_0. \tag{15}$$

Making use of the expansion (8) in Eq. (15), one has

$$U_{\text{surface}} = \int_{S_0} \left[\Gamma^{(1)}_{\alpha\beta} \varepsilon^{\text{s}}_{\alpha\beta} + \tfrac{1}{2} \Gamma^{(2)}_{\alpha\beta\kappa\lambda} \varepsilon^{\text{s}}_{\alpha\beta} \varepsilon^{\text{s}}_{\kappa\lambda} + \tfrac{1}{6} \Gamma^{(3)}_{\alpha\beta\kappa\lambda\gamma\eta} \varepsilon^{\text{s}}_{\alpha\beta} \varepsilon^{\text{s}}_{\kappa\lambda} \varepsilon^{\text{s}}_{\gamma\eta} \right] \mathrm{d}S_0, \tag{16}$$

where the surface strain is related to the bulk strain within the particle through the coordinate transformation (9). Substitution of Eq. (9) into Eq. (16) yields the strain energy stored in the surface of the ellipsoidal particle Ω when it is subjected to the bulk strain ε_{ij},

$$U_{\text{surface}} = \frac{V_0}{a} \tau_{ij} \varepsilon_{ij} + \frac{V_0}{2a} Q_{ijkl} \varepsilon_{ij} \varepsilon_{kl} + \frac{V_0}{6a} P_{ijklmn} \varepsilon_{ij} \varepsilon_{kl} \varepsilon_{mn}, \tag{17}$$

where a is the smallest of the three semi-axes of the ellipsoid and

$$\tau_{ij} = \frac{a}{V_0} \int_{S_0} \Gamma^{(1)}_{\alpha\beta} t_{\alpha i} t_{\beta j} \, \mathrm{d}S_0, \quad Q_{ijkl} = \frac{a}{V_0} \int_{S_0} \Gamma^{(2)}_{\alpha\beta\kappa\lambda} t_{\alpha i} t_{\beta j} t_{\kappa k} t_{\lambda l} \, \mathrm{d}S_0, \tag{18}$$

$$P_{ijklmn} = \frac{a}{V_0} \int_{S_0} \Gamma^{(3)}_{\alpha\beta\kappa\lambda\gamma\eta} \, t_{\alpha i} t_{\beta j} t_{\kappa k} t_{\lambda l} t_{\gamma m} t_{\eta n} \, \mathrm{d}S_0. \tag{19}$$

The fourth-order tensor Q_{ijkl} can be viewed as the *surface rigidity tensor*. It represents the combined effect of the surface stiffness, $\Gamma^{(2)}_{\alpha\beta\kappa\lambda}$, and the surface geometry. Note that the surface rigidity tensor has the dimension of force per unit length. It possesses the usual symmetry of stiffness tensors, $Q_{ijkl} = Q_{klij} = Q_{jikl} = Q_{ijlk}$. The integrals in Eqs. (18)–(19) can be further written as

$$\tau_{ij} = \frac{3}{4\pi} \int_0^{2\pi} \left[\int_0^{\pi} \Gamma^{(1)}_{\alpha\beta} t_{\alpha i} t_{\beta j} \rho \, \mathrm{d}\phi \right] \mathrm{d}\theta, \tag{20}$$

$$Q_{ijkl} = \frac{3}{4\pi} \int_0^{2\pi} \left[\int_0^{\pi} \Gamma^{(2)}_{\alpha\beta\kappa\lambda} t_{\alpha i} t_{\beta j} t_{\kappa k} t_{\lambda l} \rho \, \mathrm{d}\phi \right] \mathrm{d}\theta, \tag{21}$$

$$P_{ijklmn} = \frac{3}{4\pi} \int_0^{2\pi} \left[\int_0^{\pi} \Gamma^{(3)}_{\alpha\beta\kappa\lambda\gamma\eta} t_{\alpha i} t_{\beta j} t_{\kappa k} t_{\lambda l} t_{\gamma m} t_{\eta n} \rho \, \mathrm{d}\phi \right] \mathrm{d}\theta, \tag{22}$$

where

$$\rho = \sin\phi \sqrt{\sin^2\phi \cos^2\theta + \frac{a^2}{b^2} \sin^2\phi \sin^2\theta + \frac{a^2}{c^2} \cos^2\phi}. \tag{23}$$

It is important to observe that these tensors depend on the shape of the ellipsoid, but not the size.

It then follows from substituting Eqs. (17) and (11) into Eq. (10) that

$$U = \frac{V_0}{a} \tau_{ij} \varepsilon_{ij} + \frac{V_0}{2} \left(C_{ijkl} + \frac{1}{a} Q_{ijkl} \right) \varepsilon_{ij} \varepsilon_{kl} + \frac{V_0}{6} \left(C^{(3)}_{ijklmn} + \frac{1}{a} P_{ijklmn} \right) \varepsilon_{ij} \varepsilon_{kl} \varepsilon_{mn}. \tag{24}$$

This gives the total strain energy of the particle when it deforms relative to the undeformed perfect crystal lattice of an infinite extent.

Because of surface stresses, the self-equilibrium state of the particle is different from the perfect crystal lattice of an infinite extent. The strain tensor, $\hat{\varepsilon}_{ij}$, that describes the deformation from the perfect crystal lattice to the self-equilibrium state of the particle can be found by minimizing the total strain energy. To this end, consider

$$\left.\frac{\partial U}{V_0 \partial \varepsilon_{ij}}\right|_{\varepsilon_{ij}=\hat{\varepsilon}_{ij}} = \left(C_{ijkl} + \frac{1}{a} Q_{ijkl}\right)\hat{\varepsilon}_{kl} + \frac{1}{2}\left(C^{(3)}_{ijklmn} + \frac{1}{a} P_{ijklmn}\right)\hat{\varepsilon}_{kl}\hat{\varepsilon}_{mn} + \frac{1}{a}\tau_{ij} = 0. \tag{25}$$

This is a set of six quadratic equations which, in general, needs to be solved numerically for the six components of self-equilibrium strain tensor $\hat{\varepsilon}_{ij}$. Once $\hat{\varepsilon}_{ij}$ is found, the effective modulus tensor of the particle at the state of self-equilibrium can be defined as

$$\bar{C}_{ijkl} = \frac{\partial^2}{\partial \varepsilon_{ij} \partial \varepsilon_{kl}}\left(\frac{U}{V_0}\right)\bigg|_{\varepsilon=\hat{\varepsilon}} = C_{ijkl} + \frac{1}{a} Q_{ijkl} + \left(C^{(3)}_{ijklmn} + \frac{1}{a} P_{ijklmn}\right)\hat{\varepsilon}_{mn}. \tag{26}$$

Note that in deriving Eq. (26), it has been assumed that the strain in the ellipsoid bulk is uniform. Consequently, the effective modulus tensor given by Eq. (26) is generally an upper bound.

When the self-equilibrium strain is small, i.e., $\hat{\varepsilon}_{ij} \ll 1$, the quadratic term in Eq. (25) can be neglected. This yields the self-equilibrium strain,

$$\hat{\varepsilon}_{ij} \approx -\frac{1}{a}\left(C_{ijkl} + \frac{1}{a} Q_{ijkl}\right)^{-1} \tau_{kl}. \tag{27}$$

Substitution of Eq. (27) into Eq. (26) leads to

$$\bar{C}_{ijkl} = C_{ijkl} + \frac{1}{a} Q_{ijkl} - \frac{1}{a}\left(C^{(3)}_{ijklmn} + \frac{1}{a} P_{ijklmn}\right)\left(C_{mnpq} + \frac{1}{a} Q_{mnpq}\right)^{-1} \tau_{pq}. \tag{28}$$

This is the effective elastic modulus tensor of the particle.

Further, if one assumes

$$C_{ijkl} \gg \frac{1}{a} Q_{ijkl}, \quad C^{(3)}_{ijklmn} \gg \frac{1}{a} P_{ijklmn}, \tag{29}$$

Eqs. (27)–(28) can be simplified to obtain the explicit expressions of the self-equilibrium strain and the effective elastic modulus tensor,

$$\hat{\varepsilon}_{ij} \approx -\frac{1}{a} C^{-1}_{ijkl}\tau_{kl} = -\frac{1}{a} M_{ijkl}\tau_{kl}, \tag{30}$$

$$\bar{C}_{ijkl} = C_{ijkl} + \frac{1}{a}(Q_{ijkl} - C^{(3)}_{ijklmn} M_{mnpq}\tau_{pq}). \tag{31}$$

where $M_{ijkl} = C^{-1}_{ijkl}$ is the compliance tensor of the bulk crystal.

As mentioned earlier, Q_{ijkl} and P_{ijklmn} are independent of the particle size a. Therefore, the assumptions made in Eq. (29), for a given material, effectively place a lower limit on the particle size for which the explicit expressions (30)–(31) are valid.

All of our numerical experiments have shown that Eq. (29) is met for a as small as a few nanometers.

It is seen that the contribution of the surface energy to the effective modulus of the particle is inversely proportional to the particle size. It will be shown later numerically that the surface energy contribution is negligible unless the particle size approaches the nanometer range.

To close this section, it is worth mentioning that if the surface stiffness tensor is independent of the location, i.e., the surface is homogeneous, then the tensor Q_{ijkl} can be obtained analytically for spherical particles ($a = b = c$), wires and fibers. Their expressions are given in Appendix C.

3.1. Thin films

Consider a thin film made of a single crystal with cubic symmetry. Further, it is assumed that the top and bottom surfaces of the film are the {1 0 0} planes of the cubic crystal. In the crystallographic coordinate system shown in Fig. 4, the second- and third-order elasticity tensors of the crystal are denoted by C_{ijkl} and $C^{(3)}_{ijklmn}$, respectively. Using the Voigt notation, the non-zero, independent components of these tensors are C_{11}, C_{12} and C_{44} for C_{ijkl}, and C_{111}, C_{112}, C_{123}, C_{144}, C_{155} and C_{456} for $C^{(3)}_{ijklmn}$. The relationship between indices of the Voigt and tensorial notations is given in Appendix B. For example, $11 \to 1$, $23 \to 4$, thus, $C_{1123} = C_{14}$ and $C^{(3)}_{112323} = C_{144}$.

In this particular case, the integrals in Eq. (18) can be easily evaluated to yield the non-zero components of τ_{ij} and Q_{ijkl}

$$\tau_{22} = \tau_{33} = \Gamma_{11}, \tag{32}$$

$$Q_{2222} = Q_{3333} = K^{s} + \mu^{s}, \quad Q_{2233} = K^{s} - \mu^{s}, \quad Q_{2323} = \mu^{s}, \tag{33}$$

where Γ_{11}, K^{s} and μ^{s} are related to $\Gamma^{(1)}_{\alpha\beta}$ and $\Gamma^{(2)}_{\alpha\beta\kappa\lambda}$ as indicated in Appendix B. Substituting the above into Eq. (31) yields the effective modulus tensor. Non-zero components of the effective modulus tensor for the thin film in terms of the Voigt notation are given in Appendix C.

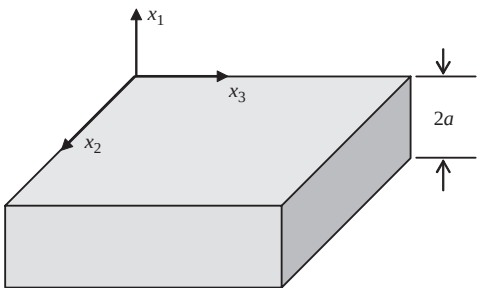

Fig. 4. A single crystal film.

It is seen from these expressions that the effective modulus tensor no longer has cubic symmetry. It becomes orthotropic. One quantity of interest is the in-plane unidirectional Young's modulus in the $\langle 1\,0\,0\rangle$ direction,

$$\bar{E}_{\langle 1\,0\,0\rangle} = \bar{E}_{22} = \bar{E}_{33} = (\bar{C}_{22} - \bar{C}_{23})\left[1 + \frac{\bar{C}_{11}\bar{C}_{23} - \bar{C}_{12}^2}{\bar{C}_{11}\bar{C}_{22} - \bar{C}_{12}^2}\right]. \tag{34}$$

Substituting Eqs. (C.4)–(C.9) into Eq. (34) and keeping terms only up to $1/a$ yields

$$\bar{E}_{\langle 1\,0\,0\rangle} = E_{\langle 1\,0\,0\rangle} + \frac{1}{a}(K^{\mathrm{s}}\kappa + \Gamma_{11}\chi), \tag{35}$$

where

$$E_{\langle 1\,0\,0\rangle} = C_{11} - \frac{2C_{12}^2}{C_{11} + C_{12}} \tag{36}$$

is the unidirectional Young's modulus of the bulk crystal in the $\langle 1\,0\,0\rangle$ directions and

$$\kappa = \frac{\mu^{\mathrm{s}}}{K^{\mathrm{s}}}\left(\frac{C_{11} + 2C_{12}}{C_{11}C_{12}}\right)^2 + \left(\frac{C_{11}}{C_{11} + C_{12}}\right)^2, \tag{37}$$

$$\chi = \frac{\eta}{(C_{11} + C_{12})^2}\left[\left(\frac{2C_{12}^3 - C_{11}^3 - 2C_{12}C_{11}^2 - 2C_{12}^2C_{11}}{C_{11}C_{12}}\right)C_{111} + \left(6C_{11} - \frac{C_{11}^2}{C_{12}} + \frac{4C_{12}^2}{C_{11}}\right)C_{112} + 2\left(C_{11} - 2C_{12} - \frac{2C_{12}^2}{C_{11}}\right)C_{123}\right]. \tag{38}$$

Clearly, κ and χ are due to surface stress and third-order elastic constants. The parameter η in the above equation is defined in Appendix C by Eq. (C.10).

The in-plane biaxial Young's modulus is defined as

$$\bar{E}_{\mathrm{b}} = \bar{C}_{22} + \bar{C}_{23} - \frac{2\bar{C}_{12}^2}{\bar{C}_{11}}. \tag{39}$$

Substituting Eqs. (C.4)–(C.9) into Eq. (39) and keeping terms only up to $1/a$ yields

$$\bar{E}_{\mathrm{b}} = E_{\mathrm{b}} + \frac{1}{a}(2K^{\mathrm{s}} + \Gamma_{11}\chi), \tag{40}$$

where

$$E_{\mathrm{b}} = \bar{C}_{11} + \bar{C}_{12} - \frac{2\bar{C}_{12}^2}{\bar{C}_{11}} \tag{41}$$

is the biaxial Young's modulus of the bulk crystal in the $\{1\,0\,0\}$ planes and

$$\chi = \eta\left[\left(\frac{4C_{12}^2}{C_{11}^3} - \frac{1}{C_{12}}\right)C_{111} + 3\left(\frac{2}{C_{11}} - \frac{1}{C_{12}} - \frac{4C_{12}}{C_{11}^2}\right)C_{112} + \frac{6}{C_{11}}\,C_{123}\right]. \tag{42}$$

Clearly, χ is due to surface stress and third-order elastic constants.

Under biaxial loading, $\sigma_{22} = \sigma_{33}$ and $\sigma_{11} = 0$, one can define an effective biaxial Poisson's ratio, $\bar{\nu}_{\mathrm{b}} = -\varepsilon_{11}/\varepsilon$, where $\varepsilon = \varepsilon_{22} = \varepsilon_{33}$ because of the cubic symmetry in

the x_2x_3-plane of the film. Making use of the above equations in conjunction with Eqs. (C.4)–(C.9), one arrives at

$$\bar{\nu}_{\mathrm{b}} = \frac{2C_{12}}{C_{11}} + \frac{2\Gamma_{11}\eta}{aC_{11}C_{12}}\left[\left(\frac{4C_{12}}{C_{11}} - 1\right)C_{112} - \frac{2C_{12}^2}{C_{11}^2}\,C_{111} - C_{123}\right], \tag{43}$$

where the first term is the biaxial Poisson's ratio for a bulk crystal.

It is noted here that when $\bar{\nu}_{\mathrm{b}}$ is assumed to be independent of the film thickness, i.e., neglecting the second term in Eq. (43), the effective biaxial Young's modulus (40) reduces to the effective biaxial modulus derived by Streitz et al. (1994a).

The self-equilibrium strain of the film follows directly from Eq. (27),

$$\hat{\varepsilon} = \frac{\Gamma_{11}\eta}{a}\begin{bmatrix} 2/C_{11} & 0 & 0 \\ 0 & -1/C_{12} & 0 \\ 0 & 0 & -1/C_{12} \end{bmatrix}. \tag{44}$$

Clearly the sign of Γ_{11} determines whether there is a negative (contraction) or positive (dilatation) relaxation of the film in the plane directions. For $C_{12} > 0$, positive Γ_{11} would yield negative in-plane strain and positive transverse stain. The same result for the in-plane self-equilibrium $\hat{\varepsilon}_{22} = \hat{\varepsilon}_{33}$ has been obtained by Streitz et al. (1994a).

3.2. Thin wire of square cross-section

Now, consider a thin wire of square cross-section made of a single crystal with cubic symmetry as shown in Fig. 5. Again, assume that the surfaces of the wire are the {1 0 0} planes of the cubic crystal. The corresponding effective modulus tensor of the wire can be directly computed from the general formulas given by Eqs. (27)–(40). The non-zero components of the effective modulus tensor are given in Appendix C, see Eqs. (C.20)–(C.25).

It is seen from Eqs. (C.20)–(C.25) that, just like in the case of the film, the effective modulus tensor becomes orthotropic. The unidirectional Young's modulus in the axial direction is given by

$$\bar{E}_{\langle 1\,0\,0\rangle} = E_{\langle 1\,0\,0\rangle} + \frac{1}{a}(K^{\mathrm{s}}\kappa + \Gamma_{11}\chi), \tag{45}$$

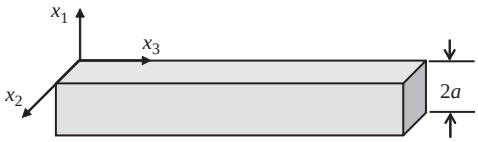

Fig. 5. A thin wire of square cross-section.

where

$$E_{\langle 1\,0\,0\rangle} = C_{11} - \frac{2C_{12}^2}{C_{11}+C_{12}} \tag{46}$$

is the unidirectional Young's modulus of the bulk crystal in the $\langle 1\,0\,0\rangle$ directions and

$$\kappa = \frac{\mu^s}{K^s}\left(\frac{C_{11}+2C_{12}}{C_{11}+C_{12}}\right)^2 + \frac{C_{11}^2+4C_{12}^2}{(C_{11}+C_{12})^2}, \tag{47}$$

$$\chi = \frac{\eta}{(C_{11}+C_{12})^2}\left[3\left(2C_{11}-4C_{12}-\frac{C_{11}^2}{C_{12}}\right)C_{112} + \left(\frac{4C_{12}^2}{C_{11}}-\frac{C_{11}^2}{C_{12}}\right)C_{111}+6C_{11}C_{123}\right]. \tag{48}$$

The Poisson's ratio is given by

$$\bar{\nu}_{13} = \bar{\nu}_{23} = \nu_{13} + \frac{1}{a}(K^s\kappa + \Gamma_{11}\chi), \tag{49}$$

where

$$\nu_{13} = \nu_{23} = \frac{C_{12}}{C_{11}+C_{12}} \tag{50}$$

is the Poisson's ratio of the bulk crystal and

$$\kappa = \frac{C_{11}}{(C_{11}+C_{12})^2} - \frac{\mu^s}{K^s}\frac{C_{11}+2C_{12}}{(C_{11}+C_{12})^2}, \tag{51}$$

$$\chi = \frac{\eta}{(C_{11}+C_{12})^2}\left[\left(1-2\frac{C_{12}}{C_{11}}\right)C_{111} + \left(4-\frac{3C_{11}}{C_{12}}-\frac{4C_{12}}{C_{11}}\right)C_{112}+\left(3-\frac{C_{11}}{C_{12}}+\frac{2C_{12}}{C_{11}}\right)C_{123}\right]. \tag{52}$$

The self-equilibrium strain is given by

$$\hat{\varepsilon} = \frac{-\Gamma_{11}\eta}{a}\begin{bmatrix} \dfrac{C_{11}-2C_{12}}{C_{11}C_{12}} & 0 & 0 \\ 0 & \dfrac{C_{11}-2C_{12}}{C_{11}C_{12}} & 0 \\ 0 & 0 & \dfrac{2}{C_{12}} \end{bmatrix}. \tag{53}$$

3.3. Spherical particles

Consider a spherical particle made of an isotropic elastic solid. Furthermore, assume that the particle's surface is homogeneous and isotropic. Clearly, this is an idealized case, for in reality a curved crystal surface inevitably involves different

crystallographic surfaces, and thus becomes non-homogeneous and anisotropic. It is nevertheless interesting to study such an idealized case because of the simplicity of the solution.

Under such assumptions, the tensors Q_{ijkl} and $R_{ijkl} = C^{(3)}_{ijklmn} M_{mnpq} \tau_{pq}$ can be easily obtained analytically by setting $a = b = c$ in the equations derived earlier. Their expressions are given in Appendix C, see Eqs. (C.26)–(C.28).

Making use of Eqs. (C.26)–(C.28), one can easily find that the effective stiffness tensor is still isotropic for an isotropic spherical particle with isotropic surface. For such a particle of radius a, the effective bulk and shear moduli are

$$\bar{K} = K + \frac{4}{3a}\left[K^{\mathrm{s}} - \frac{\Gamma_1}{K}\left(\frac{3}{2}L + 3M + \frac{4}{3}N\right)\right], \tag{54}$$

$$\bar{\mu} = \mu + \frac{1}{a}\left[\frac{1}{5}(K^{\mathrm{s}} + 6\mu^{\mathrm{s}}) - \frac{2\Gamma_1}{3K}(3M + 4N)\right], \tag{55}$$

where K and μ are, respectively, the bulk and shear moduli of the bulk material, L, M and N are the third-order elastic constants related to C_{ijk}, see Appendix B.

Making use of Eq. (27), one can compute the self-equilibrium strain of the spherical particle,

$$\hat{\varepsilon}_{ij} = -\frac{1}{a} M_{ijkl} \tau_{kl} = -\frac{2\Gamma_{11}}{3aK}\,\delta_{ij}. \tag{56}$$

This is identical to the result given by Cammarata (1997). It is seen from Eq. (56) that a positive Γ_{11} would mean a contraction of the sphere due to surface stress.

4. Numerical examples and discussion

In this section, several numerical examples for the effective modulus and effective Poisson's ratio of copper spherical particles, wires of square cross-section and films are presented. For the films and wires, it is assumed that they are made of copper single crystals and that their crystallographic directions coincide with the surfaces of the films and wires as shown in Figs. 4 and 5. The cubic (second-order) elastic constants of the copper single crystals are $C_{11} = 167.38\,\mathrm{GPa}$, $C_{12} = 124.11\,\mathrm{GPa}$. The third-order elastic constants and the surface properties are given in Table 1. For the spherical particles, the isotropic elastic properties given in Table 2 are used. The elastic properties listed in Tables 1 and 2 are taken from (Dingreville et al., 2005).

Table 1
Bulk and surface elastic constants for single crystal copper

C_{111} (GPa)	C_{112} (GPa)	C_{123} (GPa)	Γ_{11} (J/m^2)	K^{s} (J/m^2)	μ^{s} (J/m^2)
832.02	−621.92	15.29	1.3961	2.6755	−3.5524

Table 2
Bulk and surface elastic constants for polycrystal copper (isotropic)

K (GPa)	μ (GPa)	Γ_{11} (J/m^2)	K^s (J/m^2)	μ^s (J/m^2)
138.53	43.28	1.3961	2.6755	−3.5524

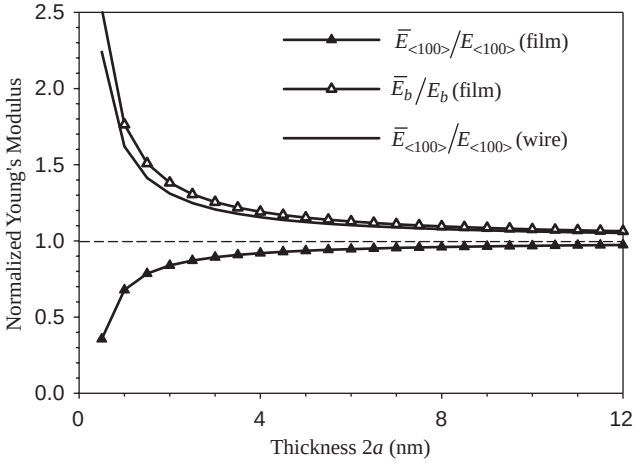

Fig. 6. Normalized effective Young's modulus of Cu films and wires of various sizes.

The effective unidirectional and biaxial moduli for single crystal Cu films and wires of various thicknesses are plotted in Fig. 6. For the wires, the axial Young's modulus increases as the wire becomes thinner. For a Cu wire with diameter of 4 nm, the axial modulus is almost 20% more than its bulk value. A similar trend is seen for the biaxial modulus of Cu films. However, the uniaxial Young's modulus for the film shows the opposite trend, i.e., it decreases with film thickness. For a 2 nm thick film, the uniaxial modulus is almost 20% less than its bulk value. Intuitively, one would think that the uniaxial Young's modulus for the film should behave more like the axial Young's modulus of the wire, because a film under uniaxial tension can be viewed as a row of many wires placed side-by-side under identical axial tension. This would be the case if the surface effect were not a factor. When the surface effect is significant, a row of wires placed side-by-side is no longer equivalent to a film because the surface area for the row of wires would be much larger.

The Poisson's ratio for the wire and the biaxial Poisson's ratio for the film are plotted in Fig. 7 for wires and films of various thicknesses. The dashed lines indicate the bulk values without the effect of free surfaces. It is seen that the bi-axial Poisson's ratio of the film decreases with decreasing film thickness, while the axial Poisson's ratio of the wire increases with decreasing wire thickness. In both cases, a sharp change occurs around thickness of 2 nm. It is interesting to note that molecular

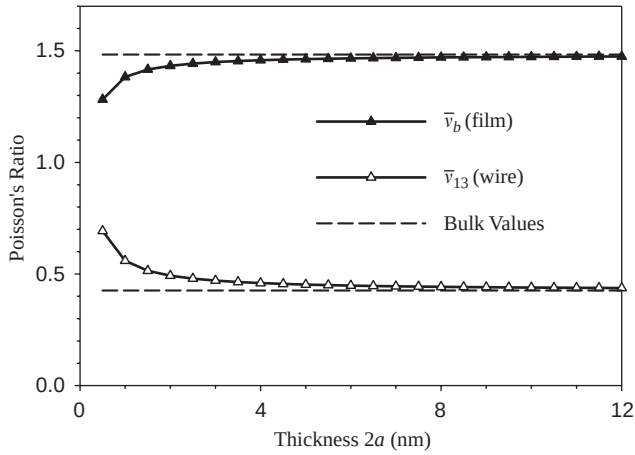

Fig. 7. Poisson's ratio for the films and the wires of various sizes.

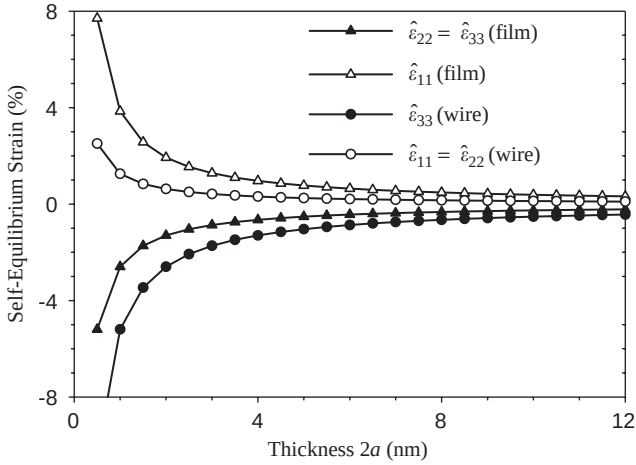

Fig. 8. Self-equilibrium strain for films and wires of various sizes.

dynamic simulations by Diao et al. (2003, 2004) have shown that single crystal gold wires undergo a phase transformation from face-centered cubic symmetry to body centered tetragonal symmetry when the wire diameter reduces to around 2 nm due to surface stress, giving rise to a significant increase in Poisson's ratio.

Plotted in Fig. 8 is the self-equilibrium strain for the films and wires. The in-plane strain for the film and the axial strain for the wire are both negative, indicating a reduction in size (area of the film, or length of the wire). This is due to the tensile surface stress for Cu in the ⟨1 0 0⟩ direction. Accompanying the size reduction is the thickness increase indicated by the positive transverse strain for both film and wire.

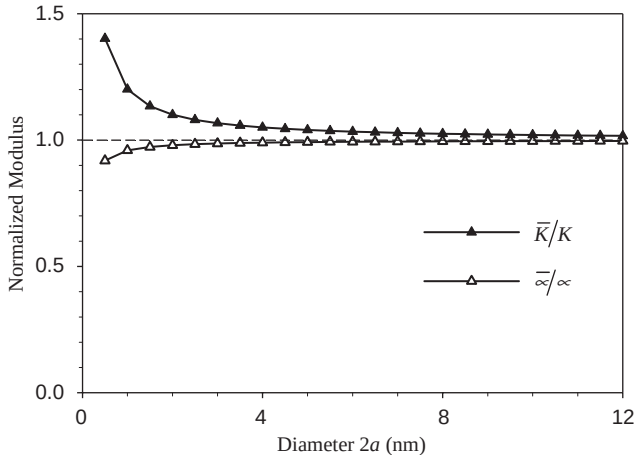

Fig. 9. Normalized effective modulus for spherical particles of various sizes.

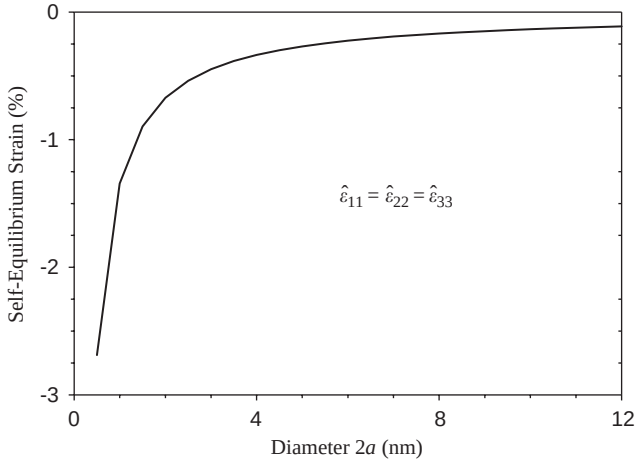

Fig. 10. Self-equilibrium strain for spherical Cu particles of various sizes.

It is noted that the self-equilibrium strain is rather significant. For example, a film of 4 nm thickness could have an in-plane shrinkage of over 0.6% and transverse expansion of almost 1%.

Now, consider a spherical particle made of isotropic elastic material with elastic properties given in Table 2. The effective shear and bulk moduli of the particle are shown in Fig. 9. It is seen that the shear modulus is much less influenced by the surface energy. The self-equilibrium strain of the particle is shown in Fig. 10. Clearly, for a Cu particle, the surface tension tends to shrink the particle. For a particle of 2 nm in diameter, the radial strain is about 1%.

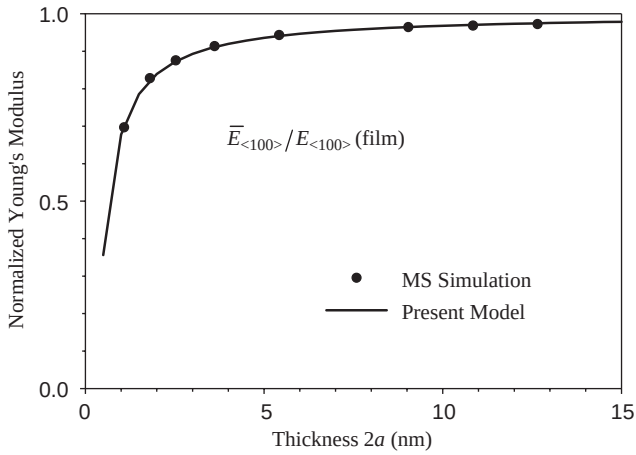

Fig. 11. Comparison of the in-plane uniaxial Young's modulus of Cu films between the results of MS simulation and the present method.

Finally, as a partial validation of the model developed here, the effective Young's modulus of thin films of various thickness was also computed using molecular static (MS) simulations. The embedded atom method was used in conjunction with the conjugate gradient method in the MS simulations. A detailed description of the MS simulation can be found in Dingreville et al. (2005). It is worth mentioning here, though, that the MS simulation is much more computationally intensive than the method developed here. The MS simulation results for the in-plane uniaxial Young's modulus are shown in Fig. 11 together with the results from the present model. It is seen that the agreement is excellent for a film as thin as 1 nm. It is also noted that the values shown in Fig. 11 also agree very well with the results by Zhou and Huang (2004) using molecular dynamic simulations and ab initio calculations.

5. Summary

In this paper, a framework is developed to incorporate the surface free energy into the continuum theory of mechanics. Analytical expressions were derived for the effective elastic modulus tensor of nano-sized structural elements that account for the effects of surface free energy. Explicit expressions of the effective elasticity tensors were obtained for thin films, wires and spherical particles. The solutions derived here show that the overall elastic properties of structural elements (such as particles, wires, films) are size-dependent. Although such size-dependency is negligible for conventional structural elements, it becomes significant when at least one of the dimensions of the structural element shrinks to nanometers. Numerical examples for copper were given in the paper to quantitatively illustrate the effects of surface free energy on the elastic properties of nano-sized particles, wires and films.

It is found that the effect of surface energy on the elastic behavior becomes significant when one of the characteristic dimensions is below about 10 nm.

Acknowledgements

The work is supported in part by the NSF Packaging Research Center at Georgia Tech. JQ was also supported in part by NSFC through Grant 10228204 and by Harbin Institute of Technology.

Appendix A. Coordinate transformation

Consider the ellipsoid Ω shown in Fig. 3. When the ellipsoid is subjected to a uniform strain field, ε_{ij}, the surface of the ellipsoid deforms accordingly. Let the two-dimensional surface strain tensor, $\varepsilon^{s}_{\alpha\beta}$, be defined in a local coordinate system $(\mathbf{i}_1, \mathbf{i}_2, \mathbf{i}_3)$, where $\mathbf{i}_1$ and $\mathbf{i}_2$ are tangent to the surface, and $\mathbf{i}_3$ is normal to the surface. Clearly, the choice of $\mathbf{i}_1$ and $\mathbf{i}_2$ is not unique. The following approach is taken to uniquely define the local coordinate system on the ellipsoidal surface.

In the spherical coordinate system,

$$x_1 = r\cos\theta\sin\phi, \quad x_2 = r\sin\theta\sin\phi, \quad x_3 = r\cos\theta, \\ 0 \leqslant \theta \leqslant 2\pi, \ \ 0 \leqslant \phi \leqslant \pi, \tag{A.1}$$

a point on the surface of the ellipsoid can be represented by the vector,

$$\mathbf{R}(\theta,\phi) = a\cos\theta\sin\phi\mathbf{I}_1 + b\sin\theta\sin\phi\mathbf{I}_2 + c\cos\phi\mathbf{I}_3. \tag{A.2}$$

A local coordinate system at this point may be introduced by the following three unit vectors:

$$\mathbf{i}_3 = \frac{1}{d_1}\left(\cos\theta\sin\phi\mathbf{I}_1 + \frac{a}{b}\sin\theta\sin\phi\mathbf{I}_2 + \frac{a}{c}\cos\phi\mathbf{I}_3\right), \tag{A.3}$$

$$\mathbf{i}_2 = \frac{\partial\mathbf{R}}{\partial\theta}\Big/\left\|\frac{\partial\mathbf{R}}{\partial\theta}\right\| = \frac{1}{d_2}\left(-\frac{a}{b}\sin\theta\mathbf{I}_1 + \cos\theta\mathbf{I}_2\right), \tag{A.4}$$

$$\mathbf{i}_1 = \mathbf{i}_2 \times \mathbf{i}_3 = \frac{a}{cd_1d_2}\cos\theta\cos\phi\mathbf{I}_1 + \frac{a^2}{bcd_1d_2}\sin\theta\cos\phi\mathbf{I}_2 - \frac{d_2}{d_1}\sin\phi\mathbf{I}_3, \tag{A.5}$$

where

$$d_1 = \sqrt{\cos^2\theta\sin^2\phi + \frac{a^2}{b^2}\sin^2\theta\sin^2\phi + \frac{a^2}{c^2}\cos^2\phi}, \tag{A.6}$$

$$d_2 = \sqrt{\frac{a^2}{b^2}\sin^2\theta + \cos^2\theta}, \tag{A.7}$$

The transformation matrix between the global $(\mathbf{I}_1, \mathbf{I}_2, \mathbf{I}_3)$ and the local $(\mathbf{i}_1, \mathbf{i}_2, \mathbf{i}_3)$ coordinate systems is thus given by

$$[t_{ij}] = \begin{bmatrix} \dfrac{a}{cd_1d_2}\cos\theta\cos\phi & \dfrac{a^2}{bcd_1d_2}\sin\theta\cos\phi & -\dfrac{d_2}{d_1}\sin\phi \\ -\dfrac{a}{bd_2}\sin\theta & \dfrac{1}{d_2}\cos\theta & 0 \\ \dfrac{1}{d_1}\cos\theta\sin\phi & \dfrac{a}{bd_1}\sin\theta\sin\phi & \dfrac{a}{cd_1}\cos\phi \end{bmatrix}. \tag{A.8}$$

Therefore, according to the tensor transformation rule, the surface strain in the local coordinate system can be written as

$$\varepsilon^{s}_{\alpha\beta} = t_{\alpha i}t_{\beta j}\varepsilon_{ij}. \tag{A.9}$$

For a spherical particle ($a = b = c$), the transformation matrix reduces to

$$[t_{ij}] = \begin{bmatrix} \cos\theta\cos\phi & \sin\theta\cos\phi & -\sin\phi \\ -\sin\theta & \cos\theta & 0 \\ \sin\phi\cos\theta & \sin\phi\sin\theta & \cos\phi \end{bmatrix}. \tag{A.10}$$

Appendix B. Bulk and surface elasticity tensors

When subjected to a strain field ε_{ij}, the strain energy of an elastic body can be written as

$$\Phi = \tfrac{1}{2}C_{ijkl}\varepsilon_{ij}\varepsilon_{kl} + \tfrac{1}{6}C^{(3)}_{ijklmn}\varepsilon_{ij}\varepsilon_{kl}\varepsilon_{mn} + \cdots, \tag{B.1}$$

where C_{ijkl} is a fourth-order tensor consisting of (second-order) elastic constants, and $C^{(3)}_{ijkl}$ is a sixth-order tensor consisting of the third-order elastic constants of the solid. It can be easily shown that the following symmetry conditions must be met by these tensors:

$$C_{ijkl} = C_{jikl} = C_{klij}, \tag{B.2}$$

$$C^{(3)}_{ijklmn} = C^{(3)}_{jiklmn} = C^{(3)}_{klmnij} = C^{(3)}_{mnijkl} = C^{(3)}_{ijmnkl} = C^{(3)}_{mnklij} = C^{(3)}_{klijmn}. \tag{B.3}$$

Instead of the tensorial notation, it is convenient in certain cases to use the Voigt (contracted) notation for these tensors. For example, C_{11} is used for C_{1111}, C_{12} is used for C_{1122}, C_{123} is used for $C_{112\,233}$, etc. The general rules to contract the indices are $(11) \to (1)$, $(22) \to (2)$, $(33) \to (3)$, $(12) \to (6)$, $(13) \to (5)$, $(23) \to (4)$. Of course, the symmetry properties of the elasticity tensor remain in their contracted form, e.g., $C_{12} = C_{21}$ and $C_{123} = C_{312}$.

For solids with cubic symmetry, there are three independent non-zero second-order elastic constants for C_{ijkl},

$$C_{11} = C_{22} = C_{23}, \quad C_{12} = C_{13} = C_{23}, \quad C_{44} = C_{55} = C_{66} \tag{B.4}$$

and six independent non-zero third-order elastic constants for $C^{(3)}_{ijklmn}$,

$$C_{111} = C_{222} = C_{333}, \quad C_{144} = C_{255} = C_{366}, \tag{B.5}$$

$$C_{112} = C_{113} = C_{122} = C_{133} = C_{223} = C_{233}, \tag{B.6}$$

$$C_{155} = C_{166} = C_{244} = C_{266} = C_{344} = C_{355}, \quad C_{123}, \quad C_{456}. \tag{B.7}$$

For isotropic solids, the number of independent elastic constants is further reduced. For C_{ijkl}, there are only two independent ones. They are

$$C_{11} = C_{22} = C_{33} = K + \frac{4\mu}{3}, \; C_{12} = C_{13} = C_{23} = K - \frac{2\mu}{3}, \tag{B.8}$$

$$C_{44} = C_{55} = C_{66} = \mu, \tag{B.9}$$

where K is called the bulk modulus, μ the shear modulus.

For isotropic solids, $C^{(3)}_{ijklmn}$ has three independent non-zero constants L, M, N. They are related to C_{ijk} by

$$C_{111} = C_{222} = C_{333} = L + 6M + 8N, \tag{B.10}$$

$$C_{144} = C_{255} = C_{366} = M, \tag{B.11}$$

$$C_{112} = C_{113} = C_{122} = C_{133} = C_{223} = C_{233} = L + 2M, \tag{B.12}$$

$$C_{155} = C_{166} = C_{244} = C_{266} = C_{344} = C_{355} = M + 2N, \tag{B.13}$$

$$C_{123} = L, \quad C_{456} = N. \tag{B.14}$$

In terms of the Kronecker delta δ_{ij}, these elasticity tensors can be written conveniently as,

$$C_{ijkl} = K\delta_{ij}\delta_{kl} + \mu\left(\delta_{ik}\delta_{jl} + \delta_{il}\delta_{jk} - \frac{2}{3}\delta_{ij}\delta_{kl}\right), \tag{B.15}$$

$$\begin{aligned} C^{(3)}_{ijklmn} = {} & L\delta_{ij}\delta_{kl}\delta_{mn} \\ & + M(\delta_{ij}\delta_{km}\delta_{ln} + \delta_{ij}\delta_{kn}\delta_{lm} + \delta_{im}\delta_{jn}\delta_{kl} + \delta_{in}\delta_{jm}\delta_{kl} + \delta_{ik}\delta_{jl}\delta_{mn} \\ & + \delta_{il}\delta_{jk}\delta_{mn}) + N(\delta_{ik}\delta_{jm}\delta_{ln} + \delta_{im}\delta_{jk}\delta_{ln} + \delta_{il}\delta_{jm}\delta_{kn} + \delta_{im}\delta_{jl}\delta_{kn} \\ & + \delta_{ik}\delta_{jn}\delta_{lm} + \delta_{in}\delta_{jk}\delta_{lm} + \delta_{il}\delta_{jn}\delta_{km} + \delta_{in}\delta_{jl}\delta_{km}). \end{aligned} \tag{B.16}$$

Next, consider the surface elasticity tensors $\Gamma^{(1)}_{\alpha\beta}$ and $\Gamma^{(2)}_{\alpha\beta\kappa\lambda}$. Again, it follows from the definition (7) that certain symmetry conditions must be met,

$$\Gamma^{(1)}_{\alpha\beta} = \Gamma^{(1)}_{\beta\alpha}, \quad \Gamma^{(2)}_{\alpha\beta\kappa\lambda} = \Gamma^{(2)}_{\kappa\lambda\alpha\beta} = \Gamma^{(2)}_{\beta\alpha\kappa\lambda}. \tag{B.17}$$

In general, $\Gamma^{(1)}_{\alpha\beta}$ and $\Gamma^{(2)}_{\alpha\beta\kappa\lambda}$ can be anisotropic in the surface (where they are defined). For isotropic surfaces, both $\Gamma^{(1)}_{\alpha\beta}$ and $\Gamma^{(2)}_{\alpha\beta\kappa\lambda}$ should be isotropic. It can be shown (Aris, 1962) that $\Gamma^{(1)}_{\alpha\beta}$ is isotropic if and only $\Gamma^{(1)}_{12} = \Gamma^{(1)}_{21} = 0$ and $\Gamma^{(1)}_{11} = \Gamma^{(1)}_{22}$, and $\Gamma^{(2)}_{\alpha\beta\kappa\lambda}$ is isotropic if and only $\Gamma^{(2)}_{1112} = \Gamma^{(2)}_{1222} = 0$, and $\Gamma^{(2)}_{1111} =$

$\Gamma^{(2)}_{2222} = \Gamma^{(2)}_{1122} + 2\Gamma^{(2)}_{1212}$. This is the case if the surface has a rotation axis of three-fold or higher symmetry (Buerger, 1963). Therefore, for a {1 1 1} surface, which has three-fold symmetry, and for a {1 0 0} surface, which has four-fold symmetry, the surface stiffness tensors can be written as

$$\Gamma^{(1)}_{\alpha\beta} = \Gamma_{11}\delta_{\alpha\beta}, \quad \Gamma^{(2)}_{\alpha\beta\kappa\lambda} = K^{s}\delta_{\alpha\beta}\delta_{\kappa\lambda} + \mu^{s}(\delta_{\alpha\kappa}\delta_{\beta\lambda} + \delta_{\alpha\lambda}\delta_{\beta\kappa} - \delta_{\alpha\beta}\delta_{\kappa\lambda}). \tag{B.18}$$

Appendix C. Special cases

C.1. Films

For the film shown in Fig. 4, the integrals in Eq. (18) can be written as integrals on the top and bottom surfaces of the film. On these surfaces, the integrands in both integrals are constants. Thus, they can be easily carried out to yield Eqs. (32) and (33). Consequently, the non-zero components of the fourth-order tensor $R_{ijkl} = C^{(3)}_{ijklmn}M_{mnpq}\tau_{pq}$ are obtained as

$$R_{1111} = 2\Gamma_{11}\eta\left(\frac{C_{112}}{C_{12}} - \frac{C_{111}}{C_{11}}\right), \quad R_{1122} = R_{1133} = \Gamma_{11}\eta\left(\frac{C_{123}+C_{112}}{C_{12}} - \frac{2C_{112}}{C_{11}}\right), \tag{C.1}$$

$$R_{2222} = R_{3333} = \Gamma_{11}\eta\left(\frac{C_{111}+C_{112}}{C_{12}} - \frac{2C_{112}}{C_{11}}\right), \quad R_{2233} = 2\Gamma_{11}\eta\left(\frac{C_{112}}{C_{12}} - \frac{C_{123}}{C_{11}}\right), \tag{C.2}$$

$$R_{2323} = 2\Gamma_{11}\eta\left(\frac{C_{155}}{C_{12}} - \frac{C_{144}}{C_{11}}\right), \quad R_{1313} = R_{1212} = \Gamma_{11}\eta\left(\frac{C_{144}+C_{155}}{C_{12}} - \frac{2C_{155}}{C_{11}}\right), \tag{C.3}$$

where C_{ijk} are related to their third-order elastic constants as indicated in Appendix B and η is defined by Eq. (C.10). The non-zero components of the effective elasticity tensor for the thin film in terms of the Voigt notation can then be obtained from Eq. (31),

$$\bar{C}_{11} = C_{11} + \frac{2\Gamma_{11}\eta}{a}\left(\frac{C_{111}}{C_{11}} - \frac{C_{112}}{C_{12}}\right), \tag{C.4}$$

$$\bar{C}_{12} = \bar{C}_{13} = C_{12} + \frac{\Gamma_{11}\eta}{a}\left(\frac{2C_{112}}{C_{11}} - \frac{C_{123}+C_{112}}{C_{12}}\right), \tag{C.5}$$

$$\bar{C}_{22} = \bar{C}_{33} = C_{11} + \frac{1}{a}\left[(K^{s}+\mu^{s}) + \Gamma_{11}\eta\left(\frac{2C_{112}}{C_{11}} - \frac{C_{111}+C_{112}}{C_{12}}\right)\right], \tag{C.6}$$

$$\bar{C}_{23} = C_{12} + \frac{1}{a}\left[(K^{s} - \mu^{s}) + 2\Gamma_{11}\eta\left(\frac{C_{123}}{C_{11}} - \frac{C_{112}}{C_{12}}\right)\right], \tag{C.7}$$

$$\bar{C}_{44} = C_{44} + \frac{1}{a}\left[\mu^{s} + 2\Gamma_{11}\eta\left(\frac{C_{144}}{C_{11}} - \frac{C_{155}}{C_{12}}\right)\right], \tag{C.8}$$

$$\bar{C}_{55} = \bar{C}_{66} = C_{44} + \frac{\Gamma_{11}\eta}{a}\left(\frac{2C_{155}}{C_{11}} - \frac{C_{144} + C_{155}}{C_{12}}\right), \tag{C.9}$$

where η is a non-dimensional constant given by

$$\eta = \frac{C_{11}C_{12}}{(C_{11} + 2C_{12})(C_{11} - C_{12})}. \tag{C.10}$$

Note that the positive definiteness of the strain energy density requires $C_{11} > |C_{12}|$. Thus, $\eta \geqslant 0$ if $C_{12} \geqslant 0$.

C.2. Wires

For the wire shown in Fig. 5, the integrals in Eq. (18) can be written as integrals on the lateral surfaces of the wire. On these surfaces, the integrands in both integrals are constants. Thus, they can be easily carried out to yield,

$$\tau_{11} = \tau_{22} = \Gamma_{11}, \quad \tau_{33} = 2\Gamma_{11}, \tag{C.11}$$

$$Q_{1111} = Q_{2222} = K^{s} + \mu^{s}, \quad Q_{3333} = 2(K^{s} + \mu^{s}), \tag{C.12}$$

$$Q_{1133} = Q_{2233} = K^{s} - \mu^{s}, \quad Q_{2323} = Q_{1313} = \mu^{s}. \tag{C.13}$$

Consequently, the non-zero components of the fourth-order tensor $R_{ijkl} = C^{(3)}_{ijklmn}M_{mnpq}\tau_{pq}$ are obtained as

$$R_{1111} = R_{2222} = \Gamma_{11}\eta\left(\frac{C_{111} + 3C_{112}}{C_{12}} - \frac{2(C_{111} + C_{112})}{C_{11}}\right), \tag{C.14}$$

$$R_{3333} = 2\Gamma_{11}\eta\left(\frac{C_{111} + C_{112}}{C_{12}} - \frac{2C_{112}}{C_{11}}\right), \tag{C.15}$$

$$R_{1122} = 2\Gamma_{11}\eta\left(\frac{C_{112} + C_{123}}{C_{12}} - \frac{2C_{112}}{C_{11}}\right), \tag{C.16}$$

$$R_{1133} = R_{2233} = \Gamma_{11}\eta\left(\frac{C_{123} + 3C_{112}}{C_{12}} - \frac{2(C_{112} + C_{123})}{C_{11}}\right), \tag{C.17}$$

$$R_{2323} = R_{1313} = \Gamma_{11}\eta\left(\frac{C_{144} + 3C_{155}}{C_{12}} - \frac{2(C_{144} + C_{155})}{C_{11}}\right), \tag{C.18}$$

$$R_{1212} = 2\Gamma_{11}\eta\left(\frac{C_{144} + C_{155}}{C_{12}} - \frac{2C_{155}}{C_{11}}\right). \tag{C.19}$$

The non-zero components of the corresponding effective elasticity tensor are thus given by

$$\bar{C}_{11} = \bar{C}_{22} = C_{11} + \frac{1}{a}\left[(K^{s} + \mu^{s}) + \Gamma_{11}\eta\left(\frac{2(C_{111} + C_{112})}{C_{11}} - \frac{C_{111} + 3C_{112}}{C_{12}}\right)\right], \tag{C.20}$$

$$\bar{C}_{33} = C_{11} + \frac{1}{a}\left[2(K^{s} + \mu^{s}) + 2\Gamma_{11}\eta\left(\frac{2C_{112}}{C_{11}} - \frac{C_{111} + C_{112}}{C_{12}}\right)\right], \tag{C.21}$$

$$\bar{C}_{12} = C_{12} + \frac{2\Gamma_{11}\eta}{a}\left(\frac{2C_{112}}{C_{11}} - \frac{C_{123} + C_{112}}{C_{12}}\right), \tag{C.22}$$

$$\bar{C}_{13} = \bar{C}_{23} = C_{12} + \frac{1}{a}\left[(K^{s} - \mu^{s}) + \Gamma_{11}\eta\left(\frac{2(C_{112} + C_{123})}{C_{11}} - \frac{3C_{112} + C_{123}}{C_{12}}\right)\right], \tag{C.23}$$

$$\bar{C}_{44} = \bar{C}_{55} = C_{44} + \frac{1}{a}\left[\mu^{s} + \Gamma_{11}\eta\left(\frac{2(C_{144} + C_{155})}{C_{11}} - \frac{C_{144} + 3C_{155}}{C_{12}}\right)\right], \tag{C.24}$$

$$\bar{C}_{66} = C_{44} + \frac{2\Gamma_{11}\eta}{a}\left(\frac{2C_{155}}{C_{11}} - \frac{C_{144} + C_{155}}{C_{12}}\right). \tag{C.25}$$

C.3. Spherical particles

$$Q_{ijkl} = \frac{4}{3}K^{s}\delta_{ij}\delta_{kl} + \frac{1}{5}(K^{s} + 6\mu^{s})\left(\delta_{ik}\delta_{jl} + \delta_{il}\delta_{jk} - \frac{2}{3}\delta_{ij}\delta_{kl}\right), \tag{C.26}$$

$$\tau_{ij} = 2\Gamma_{11}\delta_{ij}, \tag{C.27}$$

$$R_{ijkl} = \frac{2\Gamma_{11}}{3K}\left(3L + 6M + \frac{8}{3}N\right)\delta_{ij}\delta_{kl} + \frac{2\Gamma_{11}}{3K}(3M + 4N)\left(\delta_{ik}\delta_{jl} + \delta_{il}\delta_{jk} - \frac{2}{3}\delta_{ij}\delta_{kl}\right). \tag{C.28}$$

References

Ackland, G.J., Finnis, M.W., 1986. Semi-empirical calculation of solid surface tensions in B.C.C. transition metals. Philos. Mag. A 54, 301–315.

Adams, J.B., Wolfer, W.G., Foiles, S.M., 1989. Elastic properties of grain boundaries in copper and their relationship to bulk elastic constants. Phys. Rev. B 40, 9479–9484.

Alber, I., Bassani, J.L., Khantha, M., Vitek, V., Wang, G.J., 1992. Grain boundaries as heterogeneous systems: atomic and continuum elastic properties. Philos. Trans. R. Soc. London A 339, 555–586.

Alymov, M.I., Shorshorov, M.K., 1999. Surface tension of ultrafine particles. NanoStruct. Mater. 12, 365–368.

Aris, R., 1962. Vectors, Tensors, and Basic Equations of Fluid Mechanics. Prentice-Hall, Englewood Cliffs, NJ.

Baker, S.P., Small, M.K., Vlassak, B.J., Daniels, B.J., Nix, W.D., 1993. The search for the supermodulus effect. In: Nastasi, M., Parkin, D. M., Gleiter, H., (Eds.), Mechanical Properties and Deformation Behavior of Materials Having Ultra-Fine Microstructures. Kluwer Academic Publishers, Netherlands, pp. 53–67.

Banerjea, A., Smith, J.R., 1987. Continuum elasticity analysis of the enhanced modulus effect in metal–alloy superlattice films. Phys. Rev. B 35, 5413–5420.

Bassani, J.L., Vitek, V., Alber, I., 1992. Atomic-level elastic properties of interfaces and their relation to continua. Acta Metall. Mater. 40, S307–S320.

Blakely, J.M., 1973. Introduction to the Properties of Crystal Surfaces. Pergamon Press, New York.

Buerger, M.J., 1963. Elementary Crystallography. Wiley, New York (Chapter 11).

Cammarata, R.C., 1997. Surface and interface stress effects on interfacial and nanostructured materials. Mater. Sci. Eng. A 237, 180–184.

Cammarata, R.C., Sieradzki, K., 1989. Effects of surface stress on the elastic moduli of thin films and superlattices. Phys. Rev. Lett. 62, 2005–2008.

Cammarata, R.C., Sieradzki, K., 1994. Surface and interface stresses. Annu. Rev. Mater. Sci. 24, 215–234.

Cammarata, R.C., Trimble, T.M., Srolovitz, D.J., 2000. Surface stress model for intrinsic stresses in thin films. J. Mater. Res. 15, 2468–2474.

Capolungo, L., Jochum, C., Cherkaoui, M., Qu, J., 2005. Homogenization method for strength and inelastic behavior of nanocrystalline materials. Int. J. Plasticity 21, 67–82.

Capolungo, L., Cherkaoui, M., Qu, J., 2005, A self consistent model for the inelastic deformation of nanocrystalline materials. ASME J. Eng. Mater. Technol., to appear.

Catlin, A., Walter, W.P., 1960. Mechanical properties of thin single-crystal gold films. J. Appl. Phys. 31, 2135–2139.

Diao, J., Gall, K., Dunn, M.L., 2003. Surface-stress-induced transformation in metal nanowires. Nat. Mater. 2, 656–660.

Diao, J., Gall, K., Dunn, M.L., 2004. Atomistic simulation of the structure and elastic properties of gold nanowires. J. Mech. Phys. Solids 52, 1935–2186.

Dingreville, R., Qu, J., Cherkaoui, M., 2005. Calculating surface energy using molecular static simulations., in preparation.

Fartash, A., Fullerton, E.E., Schuller, I.K., Bobbin, S.E., Wagner, J.W., Cammarata, R.C., Kumar, S., Grimsditch, M., 1991. Evidence for the supermodulus effect and enhanced hardness in metallic superlattices. Phys. Rev. B 44, 13760–13763.

Fougere, G.E., Riester, L., Ferber, M., Weertman, J.R., Siegel, R.W., 1995. Young's Modulus of nanocrystalline Fe measured by nanoindentation. Mater. Sci. Eng. A 2004, 1–6.

Gibbs, J.W., 1928. The Collected Works of J. Willard Gibbs. Longmans, New York.

Gleiter, H., 1989. Nanocrystalline materials. Prog. Mater. Sci. 33, 223–315.

Gurtin, M.E., Murdoch, A.I., 1975. A continuum theory of elastic material surfaces. Arch. Rat. Mech. Anal. 57, 291–323.

Gurtin, M.E., Murdoch, A.I., 1978. Surface stress in solids. Int. J. Solids Struct. 14, 431–440.

Gurtin, M.E., Weissmuller, J., Larche, F., 1998. A general theory of curved deformable interfaces in solids at equilibrium. Philos. Mag. A 78, 1093–1109.

Itozaki, H., 1982. Mechanical properties of composition modulated copper–palladium foils. Ph. D. Thesis, Northwestern University.

Kluge, M.D., Wolf, D., Lutsko, J.F., Phillpot, S.R., 1990. Formalism for the calculation of local elastic constants at grain boundaries by means of atomistic simulation. J. Appl. Phys. 67, 2370.

Korn, D., Morsch, A., Birringer, R., Arnold, W., Gleiter, H., 1988. Measurements of the elastic constants and the specific heat and the entropy of grain boundaries by means of ultrasound. J. Phys. 49, C5–769.

Kosevich, Y.U., Kosevich, A.M., 1989. On the possibility of measuring the tensor of surface stress in thin crystalline plates. Solid State Commun. 70, 541–543.

Krstic, V., Erb, U., Palumbo, G., 1993. Effect of porosity on Young's modulus of nanocrystalline materials. Scr. Metall. Mater. 29, 1501–1504.

Marinopoulos, A.G., Vitek, V., Bassani, J.L., 1998. Local and effective elastic properties of grain boundaries in silicon. Phys. Stat. Sol. A 166, 453–473.

Miller, R.E., Shenoy, V.B., 2000. Size dependent elastic properties of nanosized structural elements. Nanotechnology 11, 139–147.

Murdoch, A.I., 1976. A thermodynamical theory of elastic material interfaces. Q. J. Mech. Appl. Math. 29, 245–275.

Nieman, G.W., Weetman, J.R., Siegel, R.W., 1991. Mechanical behavior of nanocrystalline Cu and Pd. J. Mater. Res. 6, 1012–1027.

Nix, W.D., Clemens, B.M., 1999. Crystallite coalescence: a mechanism for intrinsic tensile stresses in thin films. J. Mater. Res. 14, 3467–3473.

Nix, W.D., Gao, H., 1998. Atomistic interpretation of interface stress. Scr. Mater. 39, 1653–1661.

Pan, Z.W., Dai, Z.R., Wang, Z.L., 2001. Nanobelts of semiconducting oxides. Science 291, 1947–1950.

Pei, Z.W., Hwang, H.L., 2003. Formation of silicon nano-dots in luminescent silicon nitride. Appl. Surf. Sci. 212, 760–764.

Phillpot, S.R., Wolf, D., Gleiter, H., 1995. Molecular dynamic study of the synthesis and characterization of a fully dense, three-dimensional nanocrystalline material. J. Appl. Phys. 78, 847–860.

Sander, D., 2003. Surface stress: implications and measurements. Curr. Opin. Solid State Mater. Sci. 7, 51–57.

Schiøtz, J., Di Tolla, F.D., Jacobsen, K.W., 1998. Softening of nanocrystalline metals at very small grain sizes. Nature 391, 561–563.

Sharma, P., Ganti, S., 2003. Size-dependent Eshelby's tensor for embedded nano-inclusions incorporating surface/interface energies. Private Communications.

Shuttleworth, R., 1950. The surface tension of solids. Proc. R. Soc. London A 63, 444–457.

Streitz, F.H., Cammarata, R.C., Sieradzki, K., 1994a. Surface-stress effects on elastic properties, I: thin metal films. Phys. Rev. B 49, 10699–10706.

Streitz, F.H., Cammarata, R.C., Sieradzki, K., 1994b. Surface-stress effects on elastic properties, II: metallic multilayers. Phys. Rev. B 49, 10707–10716.

Suryanarayana, C., 1995. Nanocrystalline materials. Inter. Mater. Rev. 40, 41–64.

Vitek, V., Wang, G.J., Alber, I., Bassani, J.L., 1994. Relationship between modeling of the atomic structure of grain boundaries and studies of mechanical properties. J. Phys. Chem. Solids 55, 1147–1156.

Wolf, D., Kluge, M., 1990. Relationship between shear resistance and local atomic structure at grain boundaries in FCC metals. Scr. Metall. 24, 907–914.

Wolf, D., Lutsko, J.F., 1989. Structurally-induced elastic anomalies in a supperlattice of (0 0 1) twist grain boundaries. J. Mater. Res. 4, 1427–1443.

Wolf, D., Lutsko, J.F., Kluge, M., 1989. Physical properties of grain-boundary materials: comparison of EAM and central-force potentials. In: Vitek, V., Srolovitz, D.J. (Eds.), Atomistic Simulation of Materials: Beyond Pair Potentials. Plenum Press, New York, pp. 245–264.

Yang, F., 2004. Size dependent effective modulus of elastic composite materials: spherical nanocavities at dilute concentrations. J. Appl. Phys. 95, 3516–3520.

Zhou, L.G., Huang, H., 2004. Are surfaces elastically softer or stiffer? Appl. Phys. Lett. 84, 1940–1942.